Supporting Information Material

Table of Contents

Experimental Procedures

Materials. $AgNO_3$, $ZnSO_4 \cdot 7H_2O$, 1,2-ethanedithiol (EDT), thioanisole, anisole, triisopropylsilane (TIPS), 2-[(2-hydroxy-1,1-bis(hydroxymethyl)ethyl)amino]ethanesulfonic acid (TES), 4-(2-pyridylazo)resorcinol (PAR), nitrilodiaceticpropionic acid (NDAP), *N*-(2-hydroxyethyl)ethylenediamine-*N*,*N*′,*N*′-triacetic acid (HEDTA), *N*,*N*′-ethylenedi-(aspartic acid)trisodium salt (EDDS), *N*,*N*,*N*′,*N*′-tetrakis(2-pyridylmethyl)ethylenediamine (TPEN), ethylenedinitrilotetraacetic acid (EDTA), trans-1,2-diaminocyclohexane-*N*,*N*,*N*′,*N*′-tetraacetic acid (CDTA) and ethylene-bis(oxyethylenenitrilo)tetraacetic acid (EGTA) were purchased from Sigma-Aldrich. The 5,5′-dithiobis(2-nitrobenzoic acid) (DTNB) was purchased from TCI America. The metal-chelating resin Chelex 100® was from BioRad. The *N*,*N*-dimethylformamide (DMF), HCl were from VWR Chemicals. Acetonitrile (ACN) was from Merck Millipore. Acetic anhydrine, diethyl ether, dichloromethane (DCM) and dimethyl sulfoxide (DMSO) were from Avantor Performance Materials Poland (Gliwice, Poland). Tris(2-carboxyethyl)phosphine hydrochloride (TCEP), 1-methyl-2-pyrrolidinone (NMP), *N*,*N*,*N*,*N*-tetramethyl-*O*-(1*H*-benzotriazol-1-yl)uranium hexafluorophosphate (HBTU), trifluoroacetic acid (TFA), *N*,*N*-diisopropylethylamine (DIEA), piperidine, TentaGel S Ram and Fmoc-protected amino acids were obtained from Iris Biotech GmbH (Marktredwitz, Germany). Concentrations of zinc finger peptides were determine in two different ways that produced convergent results. One of them was based on the DTNB assay performed at 412 nm in specific reduced conditions, which allowed us determine the thiol contents and in consequence peptide concentration. The second assay was based on spectroscopic titration of ZF peptides with known concentrations of Zn(II) and observation of LMCT band formation which is known as a quantitative method. During spectroscopic titrations of ZF with Zn(II), TCEP was used as a non-metal binding reducing agent. The concentration of the stock solutions of the metal ion salts were 0.05 M and then confirmed by representative series of ICP-MS measurements. To eliminate trace metal ion contamination all pH buffers were treated with Chelex 100® resin and degassed over 2 h prior use. 20 mM PAR stock solution in DMSO was prepared freshly before each experiment and were not stored at room temperature longer than one week due to degradation.[1]

Peptide Synthesis. All investigated zinc finger peptides were synthesized via solid phase synthesis on TentaGel S Ram resin (substitution 0.22 mmol/g) using Fmoc-strategy and Liberty 1 microwave-assisted synthesizer (CEM). The reagent excess, cleavage and purification were performed as previously described.[2,3] The acetic anhydrate was used for N-terminal acetylation then peptides were cleaved from the resin with a mixture of TFA/anisole/thioanisole/EDT/TIPS (88/2/3/5/2 v/v/v/v/v) over a period of 2.5 h followed by precipitation in cold (-70°C) diethyl ether. The crude peptide was collected by centrifugation, dried and purified via HPLC (Waters 2487) on Phenomenex C18 columns using a gradient of ACN in 0.1% TFA/water from 0% to 40% over 20 min. The purified peptides were identified by ESI mass API 2000 Applied Biosystems spectrometry. The identified and calculated monoisotopic masses are listed in the Table S1. Polyalanine standard peptides for IMS-MS were synthesized as above with Prelude synthesizer (Protein Technologies) and TFA/TIPS/H_2O (95:5:5 v/v/v) mixture was used for cleavage. After drying they were dissolved in neat TFA and desalted by HPLC gradient from 0 to 90% over 5 min.

Circular Dichroism. CD spectra of zinc finger peptides were recorded on J-1100 Jasco spectropolarimeter at 25°C temperature in a 2 mm quartz cuvette under constant nitrogen flow over the range of 198 – 400 nm with 100 nm/min speed scan. Final spectra were averaged from 3 independent scans. The spectroscopic titration of 25 μM peptide with Zn(II) were performed in degassed and chelexed 20 mM TES buffer (pH 7.0) with the

addition of 10 mM TCEP to its final concentration of 200 μM as non-metal binding cysteine thiols protector.[4] The spectroscopic titration of 25 μM peptide with Ag(I) were performed in degassed and chelexed 20 mM TES buffer (pH 7.0) without the addition of 10 mM TCEP to avoid AgCl precipitation. All samples were equilibrated over 2 min after the addition of each portion of 2 mM $ZnSO_4$ or $AgNO_3$ solution. All CD spectra and analyzed data were presented as molar ellipticity in $deg \cdot cm^2 \cdot dmol^{-1}$.[5,6]

UV-Vis spectroscopy. UV-Vis spectra were recorded on Jasco V-650 spectrophotometer at 25°C temperature in a 1 cm quartz cuvette over the range of 200-800 nm. The spectroscopic titration of 25 μM peptides were performed in degassed and chelexed 20 mM TES buffer (pH 7.0) with Ag(I) as well as Zn(II) ions to its final concentration of 100 μM. The samples were equilibrated over 2 min after the addition of each portion of 2.5 mM metal ion solution.[7] The spectra were recorded under argon atmosphere.

***PAR monitored Zn(II) release from CP1 ZFs*.** The transfer of Zn(II) from CP1 ZFs to PAR during Ag(I) titration was performed spectrophotometrically using a Jasco V-650 spectrophotometer (JASCO) in kinetic mode at 25°C in a 1 cm quartz cuvette at a fixed wavelength of 492 nm over 3600 s. The spectroscopic titration of 10 μM peptides were performed in degassed and chelexed 20 mM TES buffer (pH 7.0), in the presence of 100 μM PAR, with Ag(I) ions to its final concentration of 10 μM. The samples were equilibrated until appearing curve, connected with Zn(II) to PAR transfer, reached plateau. The exact concentration of Zn(II) complexes with PAR was calculated based on actual absorbances at 492 nm for PAR using appropriate effective molar absorption coefficient at pH 7.0 (60,800 $M^{-1} \cdot cm^{-1}$).[1]

Stability study – competition CN^-. All measurements were recorded on J-1100 Jasco spectropolarimeter at 25°C temperature in a 2 mm quartz cuvette under constant nitrogen flow under kinetic mode over 30s at specified wavelength 220, 223, 225 nm characteristic for each ZF CP1 (CCCC), CP1 (CCCH) and CP1 (CCHH), respectively. Final point at each Ag(I) / KCN ratio was averaged from 3 independent scans. The spectroscopic titration of 25 μM peptide with Ag(I) ions in the presence of 150 μM KCN were performed in degassed and chelexed 20 mM TES buffer (pH 7.0). All samples were equilibrated over 2 min after the addition of each portion of $AgNO_3$ solution. Method of stability constant calculation is presented below.

ZFs competition with complexones. In order to determine Zn(II)-to-ZF affinity, peptides at 25 μM concentrations were equilibrated in a 1.0 mM solution of various chelators (complexones) (TPEN, CDTA, EDTA, HEDTA, EDDS, EGTA and NDAP) with 0.1-0.9 mM Zn(II) (metal buffers) over a period of 12 h.[8,9] Metal buffer sets were prepared in chelexed 20 mM TES buffer (pH. 7.0). The equilibrated samples were measured in a 2 mm quartz cuvette at a fixed wavelength of ~220 nm, which slightly differed for each peptide in order to obtain the highest possible dynamic range of ellipticity changes. The samples were measured in kinetic mode in order to obtain 30 independent measurements, which were subsequently averaged to final values. The amount of Zn(II) transferred from the metal buffer component to a particular ZF peptide was considered during recalculating final free Zn(II) values. All $-\log[Zn(II)]_{free}$ (pZn) calculations were performed based on previously established dissociation constants of Zn(II) complexes with complexones using HySS software.[10,11] All experimental points recorded for each ZF were fitted to Hill's equation.[3,7,9]

ESI-MS monitored titration of apo-CP1 ZFs with Ag(I). The ESI-MS Ag(I) titration study was performed in degassed 5 mM ammonium acetate solution (pH 7.0). A solution of 10 mM apo-ZFs was mixed with 0–4 molar

equivalents of 50 mM $AgNO_3$ solution and ammonium acetate solution was added to a final volume of 200 ml. The samples were incubated for 30 s and injected by a syringe pump (40 ml/min flow rate) into an ESI Q-ToF Premier mass spectrometer (Waters). MS spectra were recorded in positive ion mode during 5 min in the range *m/z* of 500–1800. Obtained mass spectrometry data were analyzed and processed using MassLynx (Version 4.1, Waters Inc.). All ZFs samples were prepared and stored in an anaerobic chamber.

Mass spectrometry (MS/MS experiment). MS/MS experiments were performed on an ESI Q-ToF Premier mass spectrometer (Waters). Samples were prepared in 5 mM ammonium acetate solution (pH 7.0). The experimental settings were as follows 2.5 kV capillary voltage, 30 V sampling cone, 3 V extractor cone, 80°C source temperature, 1 V trap collision energy. Transfer collision energy for Ag_2Cys_2 and Ag_3Cys_3 was 45eV, and for Ag_4Cys_4 was 50eV.

Ion mobility. MS experiments were performed using a Synapt G2 HDMS instrument (Waters). Ions were generated using nanoelectrospray ionization at 1.7 kV from PicoTip emitters 2 µm i.d. (QT10-70-2-CE-20 New Objective). MS settings were adjusted to obtain an optimal ion transmission as follows: 30 V sampling cone, 5 V extractor cone, 40°C source temperature, 10 V trap collision energy, and 5V transfer collision energy, wave height and wave velocity were set as 40 V and 800 m/s respectively. As a standard Poly-alanine peptides were used, dissolved at ~ 25 µg/mL in 1:1 acetonitrile/water (Fisher Scientific) with 0.1% formic acid.[12] Peptides were dissolved at 5 mM ammonium acetate at 25 µM concentration. Drift times were obtained for each sample by generating an extracted ion chromatogram (XIC) from the arrival time distribution function in MassLynx v4.1 using the monoisotopic mass and a mass window of ±0.075 Da. Each measurement for Poly-Ala standards and samples was repeated at least 5 times. The CCS values of Poly-Ala for calibration curves were derived from Bush *et al*.[13] The calibration curves (logarithmic fit and linear fit) were generated according to previous reports.[12,14-16] Theoretical CCS values were calculated using IMPACT software which used the projection approximation algorithm.[17] A CCS distribution was calculated from the trajectories obtained from MD simulations.

Molecular dynamics (MD) simulations. To date there is no solved structure for the zinc finger consensus and thus, homology modeling was employed to obtain the initial coordinates for molecular dynamics simulations. For this, the NMR structure of consisting in the region 760-792 of the human zinc finger protein 347 (PDB:2YTR) and the protein sequence of CP1 were fed to MODELLER 9.11.[18] The sequence identity between both was found to be around 75 %. DOPE (Discrete optimized protein energy) was selected as a metric to select the best model for subsequent MD simulations. All the MD simulations were performed with AMBER 16 software and AMBER ff99SB force field.[19] Proteins were solvated in a cubic box of 8 angstrom buffer of TIP3P water molecules. Default protonation states were used for protein residues and Cl- counterions were added to achieve electrical neutrality. The systems were subjected to 10,000 steps of energy minimization with steepest descent algorithm, followed by heating the system over 200 ps to reach 300 K temperature (NVT ensemble). Systems were further equilibrated by 2 ns for isobaric isothermal ensemble (NPT) at 300 K. A time step of 2 fs was employed for every case. SHAKE algorithm was utilized to constraint covalent bonds involving hydrogen atoms. Particle mesh Ewald method was used for calculate the long-range electrostatic interactions and the temperature of the system was maintained with Langevin dynamics with a 1 ps-1 collision frequency. Productions runs were performed under NPT ensemble at 300 K for 100 ns using harmonic potentials of strength 10 kcal/mol/Å which were imposed between S atoms of Cys residues and Ag(I)

ions to restraint a coordination distance of 2.5 Å. Final structures obtained by constraint MD were used to perform semiempirical QM/MM simulations for 1 ns. Average structures were obtained from the last 100 ps. The QM region was described with semiempirical PM6 that included the Cys residues and Ag(I) ions, and respectively water molecules. The QM/MM boundary crossed the Cα-Cβ bonds of the Cys residues and was saturated with link hydrogen atoms. Solvent molecules were kept frozen over the course of the simulation.

Well-Tempered Metadynamics (WT-MetaD) Simulations. Simulations of the Ag_4ZF protein have been carried out using GROMACS version 4.5.3 and the PLUMED plugin version 2.0.[20,21] Figures have been prepared with UCSF Chimera and the R-package metadynminer.[22] Averaged final coordinates obtained through QM/MM simulations were used as initial structure for WT-MetaD.[23] The parmed tool was used to create the topology using the AMBER99-SB force field. The initial conformation was energy minimized by 5000 steps of steepest descent and then equilibrated at 300 K by 1 ns simulation in the isothermal ensemble (NVT) followed by 1 ns simulation at 300 K and 1 atm in the isothermal-isobaric ensemble (NPT). Study of folding landscapes by MetaD is not a trivial process since involve many degrees of freedom and time scales to simultaneously bias and thus proper collective variables (CV) were chosen after many trials. The 2 CV that capture metal-coupled folding landscape were (i) the radius of gyration of the hydrophobic core characterized by side chain carbon atoms from Tyr1, Phe10 and Leu16 residues (R_g) and (ii) the second CV describes the distance root-mean-square deviation (DRMSD) with respect folded structure. The WT-MetaD bias potential was constructed using an initial deposition rate equal to 0.6 kcal/mol every 250 ps. Each Gaussian has a width equal to 0.5 for both CVs. The well-tempered bias factor was set to 10. The simulation time accomplished for ~ 1.3 μs when it showed free diffusion along the CVs. Convergence of the simulation was estimated by calculating the free energy surface (FES) as a function of time. It was selected relevant regions in the CV that corresponds to identified free energy minima and calculating free-energy differences between pairs of them as a function of simulation time. Unbiased probability distributions were obtained for a set of CVs through a reweighting procedure. CVs selected were $S\alpha$, S_{hc}, N_{nl}. S_α describes the number of backbone-backbone α-helical hydrogen bonds formed between Ser15-Cys19. S_{hc} is defined as the number of contacts in the hydrophobic core formed by Tyr1, Phe10 and Leu16. N_{nl} is the number of native coordination bonds formed between Cys residue and Ag(I).

Results

a)

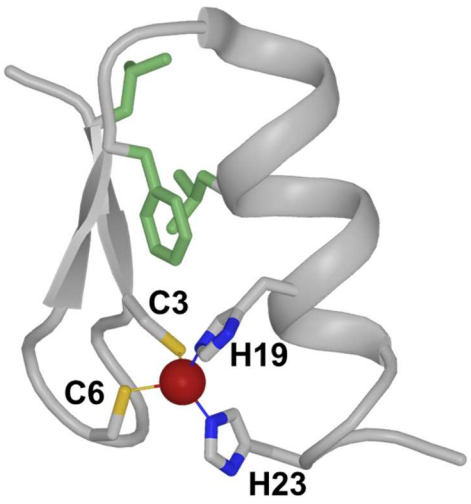

b)

CP1(2015)_variants

CCHH	Ac-YKCKECGKAFSQSSSLTRHQRIHTG-NH_2
CCCH	Ac-YKCKECGKAFSQSSSLTRCQRIHTG-NH_2
CCCC	Ac-YKCKECGKAFSQSSSLTRCQRICTG-NH_2
CCAA	Ac-YKCKECGKAFSQSSSLTRAQRIATG-NH_2
CCCA	Ac-YKCKECGKAFSQSSSLTRCQRIATG-NH_2

Figure S1. Structure of the classical ββα zinc finger and sequences of consensus peptide 1 (CP1) variants used in this study. (a) The NMR structure of the Sp1-3 zinc finger (PDB: 1VA3) as an example. (b) Sequences of the CP1 variants investigated herein.

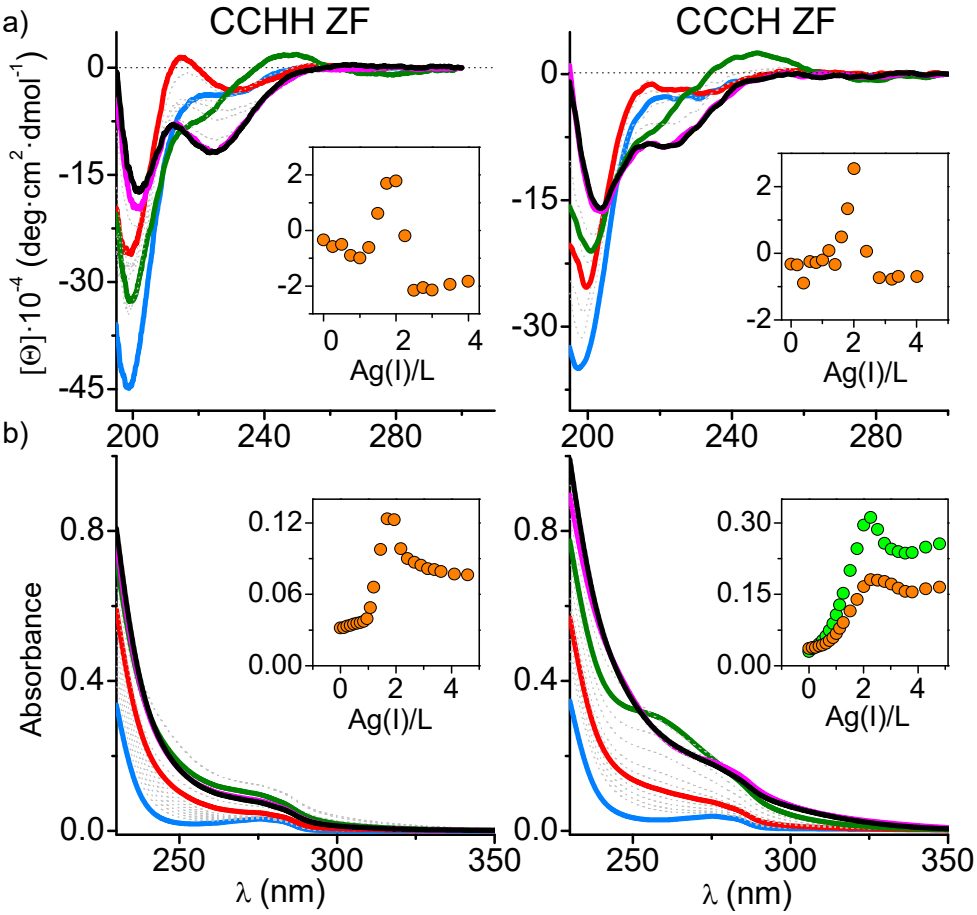

Figure S2. Spectroscopic titrations of 25 μM ZF peptides in 20 mM TES buffer (pH 7.0) with 0 eq. (blue), 1 eq. (red), 2 eq. (green), 3 eq. (magenta) and 4 eq. (black) of Ag(I). (a) Spectropolarimetric titration spectra recorded for ZF peptides. The inset show the changes in molar ellipticity at 247 nm over the range of 0-4 eq. of Ag(I). (b) Spectrophotometric spectra recorded in the UV-Vis range (230–350 nm). The inset show the changes in absorption at 260 nm (green) and 279 nm (orange) over the range of 0-4 eq. of Ag(I).

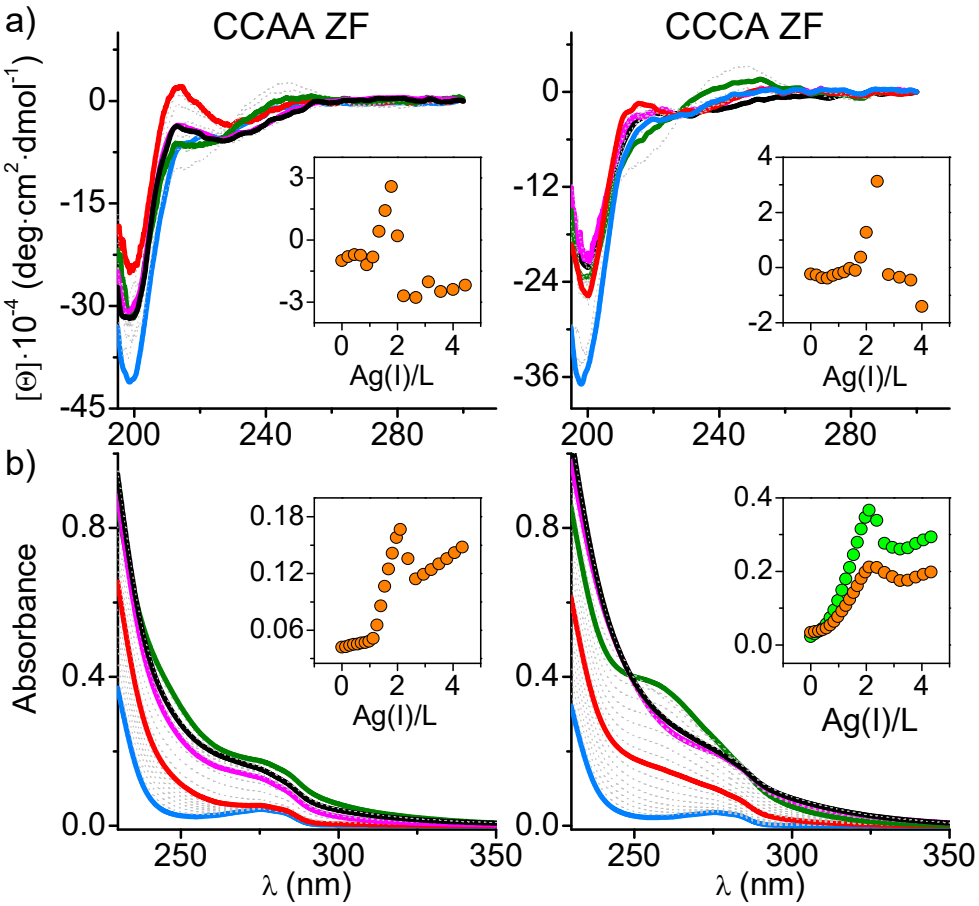

Figure S3. Spectroscopic titrations of 25 μM mutated ZF peptides (L) in 20 mM TES buffer (pH 7.0) with 0 eq. (blue), 1 eq. (red), 2 eq. (green), 3 eq. (magenta) and 4 eq. (black) of Ag(I). (a) Spectropolarimetric titration spectra recorded for ZF alanine mutants. The inset show the changes in molar ellipticity at 247 nm over the range of 0-4 eq. of Ag(I). (b) Spectrophotometric spectra recorded in the UV-Vis range (230–350 nm). The inset show the changes in absorption at 260 nm (green) and 279 nm (orange) over the range of 0-4 eq. of Ag(I).

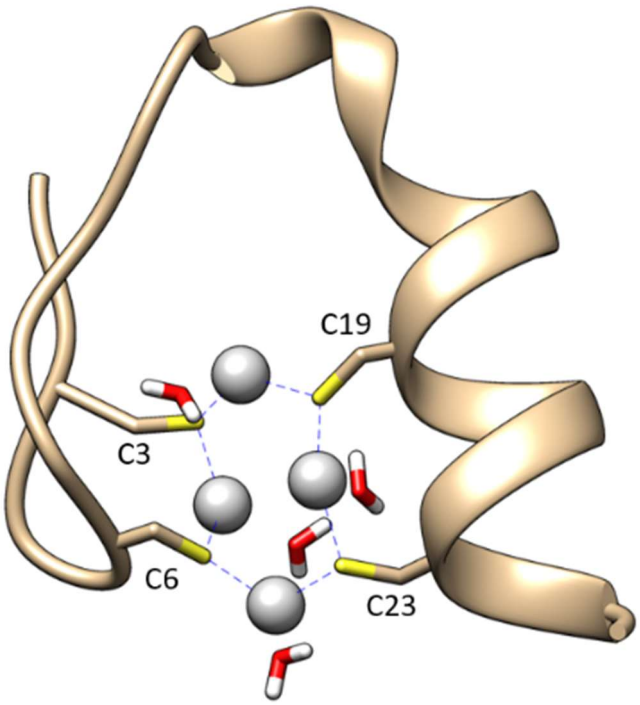

YKC_3KEC_6GKAFSQSSSLTRC_{19}QRIC_{23}TG

Figure S4. QM/MM MD-based structure of Ag_4L complex of CCCC ZF with highlighted Cys binding residues and water molecules.

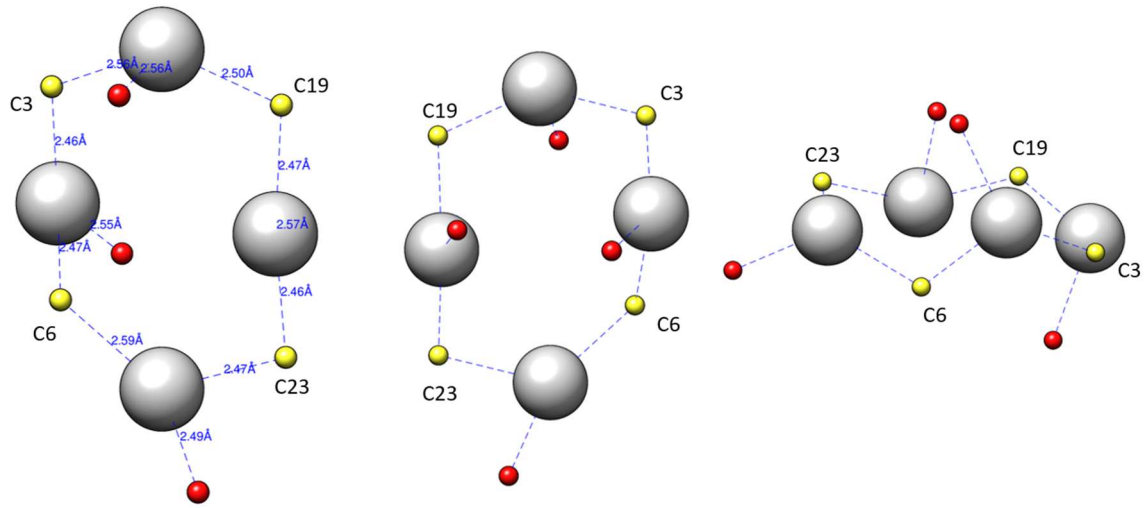

Figure S5. Visualization of the Ag_4Cys_4 cluster obtained for Ag_4L complex with CCCC ZF through QM/MM MD simulations. Grey, red and yellow circles denote Ag(I), sulfur and oxygen atoms, respectively.

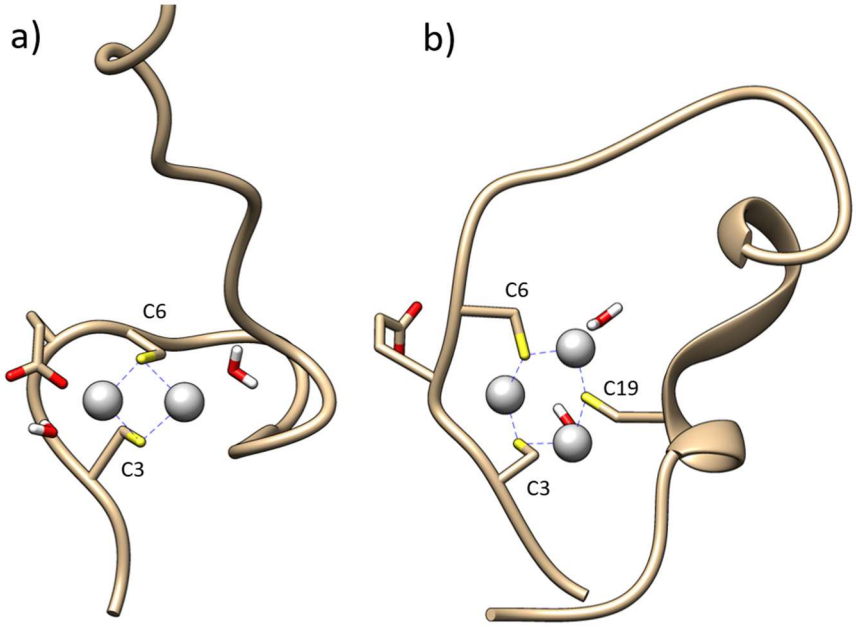

Figure S6. QM/MM MD-based structure of (a) Ag_2L of CCHH ZF and (b) Ag_3L of CCCH ZF with highlighted binding residues and water molecules.

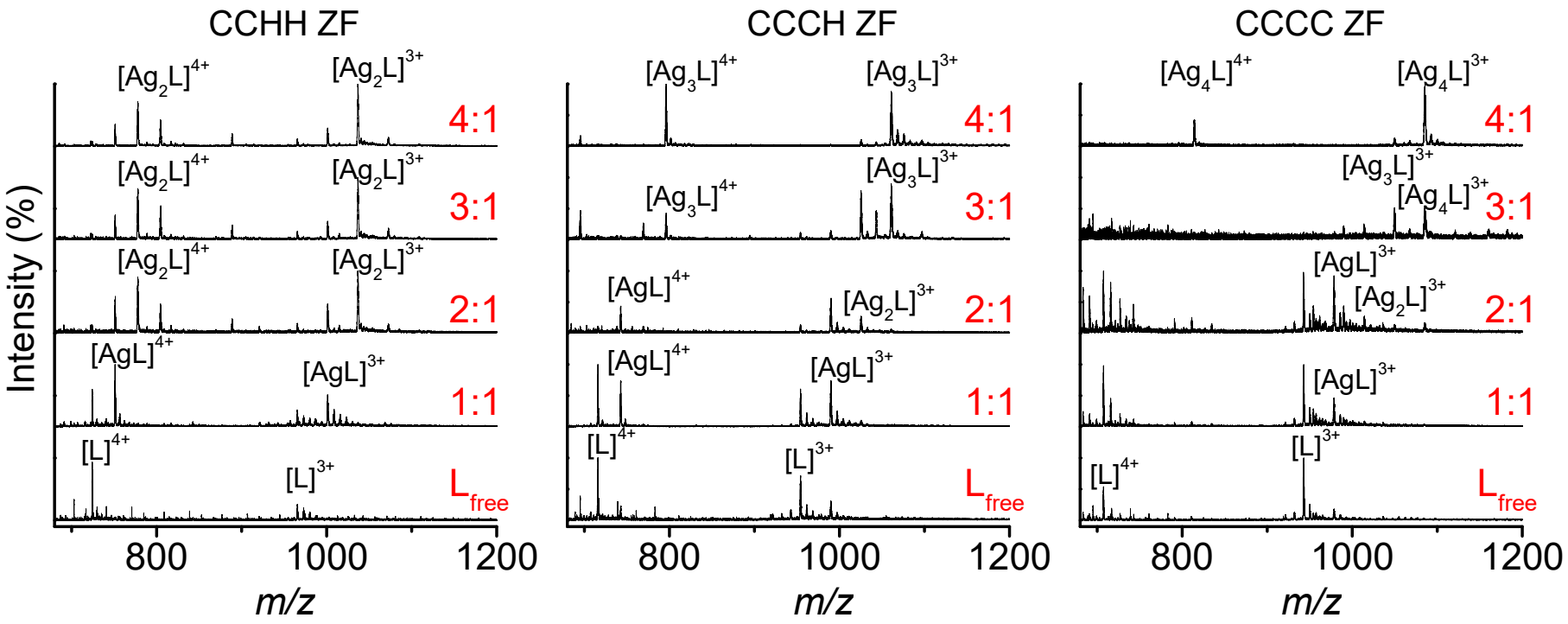

Figure S7. ESI-MS monitored Ag(I) binding. Positive-ion ESI mass spectra of ZF peptides with 0-4 eq. of Ag(I) measured in 5 mM ammonium acetate (pH 7.0) in the range *m/z* 680 – 1200. Others repeating peaks as well as those indicating adducts were not assigned in order to make this figure readable.

Table S1. List of calculated and found *m/z* values for ZF peptides (signal +3) titrated with Ag(I) ion on ESI-MS. All calculated and experimental *m/z* refers to average not monoisotopic values.

ZF peptide (L)	$[L]^{3+}$	$[AgL]^{3+}$	$[Ag_2L]^{3+}$	$[Ag_3L]^{3+}$	$[Ag_4L]^{3+}$
CCHH	965.78[a]	1001.44[a]	1037.44[a]	1073.10[a]	1108.77[a]
	965.87[b]	1001.44[b]	1037.06[b]	1072.50[b]	-
CCCH	954.44[a]	990.44[a]	1026.11[a]	1061.77[a]	1097.44[a]
	954.65[b]	990.01[b]	1026.07[b]	1061.25[b]	-
CCCC	943.11[a]	979.11[a]	1014.77[a]	1050.44[a]	1086.11[a]
	943.02[b]	978.86[b]	1014.51	1050.18	1086.00
CCAA	921.73[a]	957.73[a]	993.40[a]	1029.06[a]	1064.73[a]
	921.23[b]	957.10[b]	992.97[b]	-	-
CCCA	932.42[a]	968.42[a]	1004.10[a]	1039.75[a]	1075.42[a]
	932.01[b]	967.90[b]	1003.73[b]	1039.40[b]	-

[a] calculated *m/z;*
[b] experimental *m/z*

Table S2. MS/MS fragmentation of the +3 and +4 species obtained for CCHH ZF metal free peptide (L) and its silver complex (Ag_2L), respectively. All calculated and experimental *m/z* refers to average not monoisotopic values.

$[L]^{3+}$ = 965.632

Cal. *m/z*	Exp. *m/z*	Fragments	Type
847.464	847.698	HQRIHTG	$[y7]^{1+}$
847.446	847.698	SQSSSLTRHQRIHTG	$[y15]^{2+}$
920.980	921.685	FSQSSSLTRHQRIHTG	$[y16]^{2+}$
956.498	956.726	AFSQSSSLTRHQRIHTG	$[y17]^{2+}$
1049.057	1049.689	GKAFSQSSSLTRHQRIHTG	$[y19]^{2+}$
1100.561	1101.132	CGKAFSQSSSLTRHQRIHTG	$[y20]^{2+}$
1165.083	1165.318	ECGKAFSQSSSLTRHQRIHTG	$[y21]^{2+}$
1229.130	1229.306	KECGKAFSQSSSLTRHQRIHTG	$[y22]^{2+}$
1280.6346	1280.903	CKECGKAFSQSSSLTRHQRIHTG	$[y23]^{2+}$
437.185	437.273	YKC	$[b3]^{1+}$

$[Ag_2L]^{4+}$ = 778.01

Cal. *m/z*	Exp. *m/z*	Fragments	Type
847.464	847.698	HQRIHTG	$[y7]^{1+}$
847.446	847.698	SQSSSLTRHQRIHTG	$[y15]^{2+}$

Table S3. MS/MS fragmentation of the +3 and +4 species obtained for CCCH ZF metal free peptide (L) and its silver complex (Ag_3L), respectively. All calculated and experimental *m/z* refers to average not monoisotopic values.

$[L]^{3+}$ = 965.632

Cal. *m/z*	Exp. *m/z*	Fragments	Type
813.415	813.566	CQRIHTG	$[y7]^{1+}$
679.360	679.466	SSLTRHQRIHTG	$[y12]^{2+}$
722.876	723.003	SSSLTRHQRIHTG	$[y13]^{2+}$
786.905	787.049	QSSSLTRHQRIHTG	$[y14]^{2+}$
830.421	830.566	SQSSSLTRHQRIHTG	$[y15]^{2+}$
903.955	904.614	FSQSSSLTRHQRIHTG	$[y16]^{2+}$
939.474	939.648	AFSQSSSLTRHQRIHTG	$[y17]^{2+}$
437.185	437.237	YKC	$[b3]^{1+}$
1053.486	1053.737	YKCKECGKA	$[b9]^{1+}$

$[Ag_3L]^{4+}$ = 778.01

Cal. *m/z*	Exp. *m/z*	Fragments	Type
722.876	722.993	SSSLTRCQRIHTG	$[y13]^{2+}$

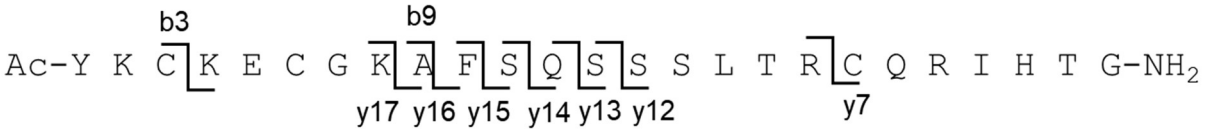

Table S4. MS/MS fragmentation of the +3 species obtained for CCCC ZF metal free peptide (L) and its silver complex (AgL). All calculated and experimental *m/z* refers to average not monoisotopic values.

$[L]^{3+}$ = 965.632

Cal. *m/z*	Exp. *m/z*	Fragments	Type
676.356	676.465	CQRICTG	$[y6]^{1+}$
662.335	662.458	SLTRCQRICTG	$[y12]^{2+}$
705.851	705.964	SSLTRCQRICTG	$[y13]^{2+}$
769.880	770.016	QSSSLTRCQRICTG	$[y14]^{2+}$
813.400	813.545	SQSSSLTRCQRICTG	$[y15]^{2+}$
886.930	887.008	FSQSSSLTRCQRICTG	$[y16]^{2+}$
922.449	922.602	AFSQSSSLTRCQRICTG	$[y17]^{2+}$

$[AgL]^{3+}$ = 978.01

Cal. *m/z*	Exp. *m/z*	Fragments	Type
1015.007	1015.177	GKAFSQSSSLTRHQRIHTG	$[y19]^{2+}$
1066.512	1067.229	CGKAFSQSSSLTRHQRIHTG	$[y20]^{2+}$

No fragmentation for signals with 2, 3 and 4 Ag(I).

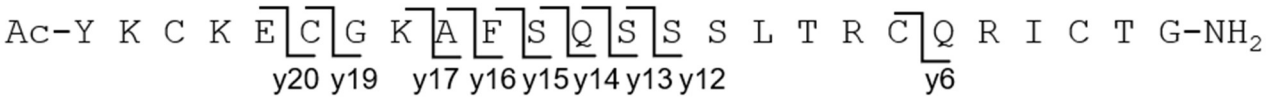

Table S5. MS/MS fragmentation of the +4 and +3 species obtained for CCAA ZF metal free peptide (L) and its silver complex (Ag_2L), respectively. All calculated and experimental *m/z* refers to average not monoisotopic values.

$[L]^{4+}$ = 691

Cal. *m/z*	Exp. *m/z*	Fragments	Type
630.363	630.484	SLTRAQRIATG	$[y12]^{2+}$
673.879	674.015	SSLTRAQRIATG	$[y13]^{2+}$
737.908	738.063	QSSSLTRAQRIATG	$[y14]^{2+}$
781.424	781.566	SQSSSLTRAQRIATG	$[y15]^{2+}$
854.958	855.629	FSQSSSLTRAQRIATG	$[y16]^{2+}$
890.477	890.623	AFSQSSSLTRAQRIATG	$[y17]^{2+}$

$[Ag_2L]^{3+}$ = 993

Cal. *m/z*	Exp. *m/z*	Fragments	Type
854.958	855.576	FSQSSSLTRAQRIATG	$[y16]^{2+}$
890.477	890.656	AFSQSSSLTRAQRIATG	$[y17]^{2+}$
983.035	983.682	GKAFSQSSSLTRAQRIATG	$[y19]^{2+}$

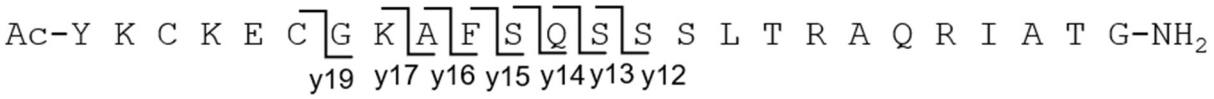

Table S6. MS/MS fragmentation of the +3 species obtained for CCCA ZF metal free peptide (L) and its silver complex (Ag_3L). All calculated and experimental *m/z* refers to average not monoisotopic values.

$[L]^{3+}$ = 965.632

Cal. *m/z*	Exp. *m/z*	Fragments	Type
689.865	689.921	SSLTRCQRIATG	$[y13]^{2+}$
753.894	755.037	QSSSLTRCQRIATG	$[y14]^{2+}$
797.410	797.564	SQSSSLTRCQRIATG	$[y15]^{2+}$
870.944	871.592	FSQSSSLTRCQRIATG	$[y16]^{2+}$
906.463	906.631	AFSQSSSLTRCQRIATG	$[y17]^{2+}$

$[Ag_3L]^{3+}$ = 1039

Cal. *m/z*	Exp. *m/z*	Fragments	Type
502.775	503.013	TRCQRIATG	$[y9]^{2+}$

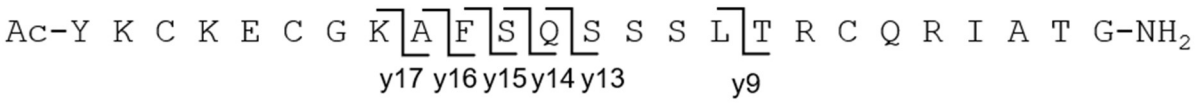

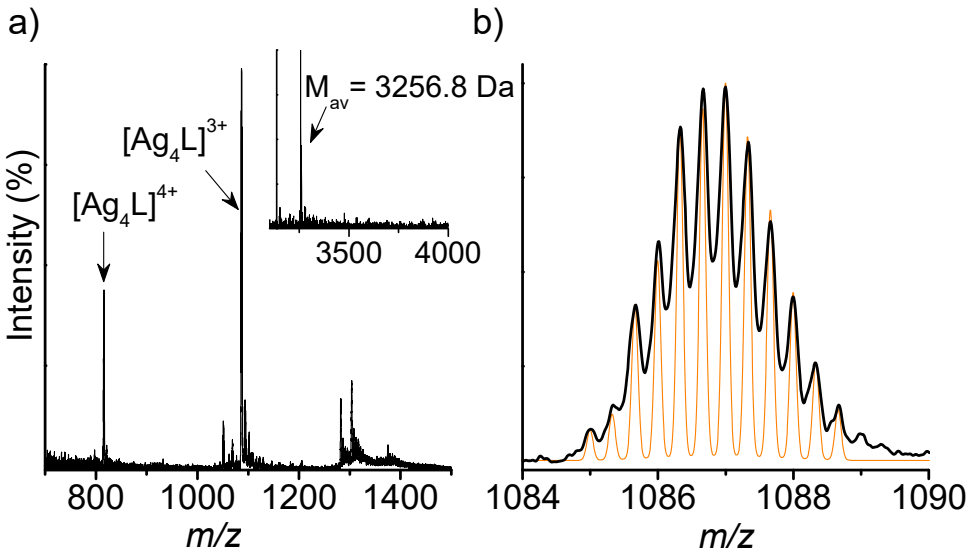

Figure S8. (a) Positive-ion ESI mass spectra of CCCC ZF with 4 eq. of Ag(I). The insert show deconvoluted ESI mass spectra for Ag_4L. (b) Isotopic pattern of $[Ag_4L]^{3+}$ ion from experimental (black) and simulated (orange).

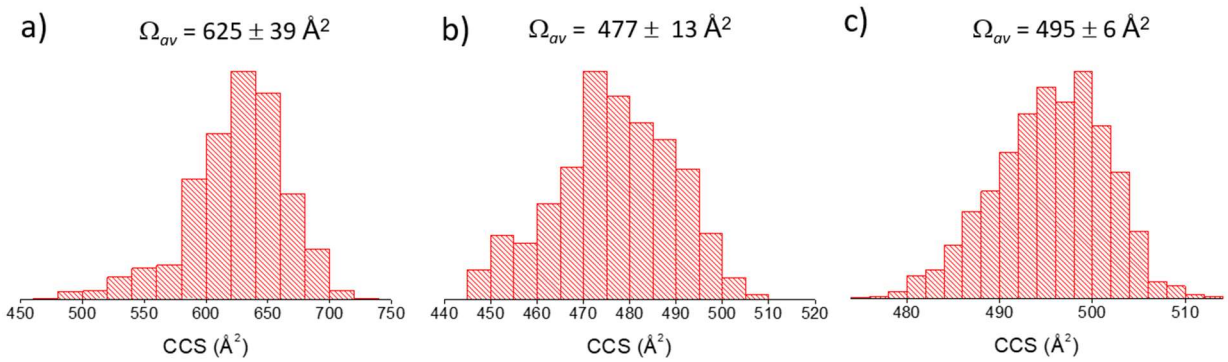

Figure S9. Collision cross sections (CCS) calculated with IMPACT software for the MD trajectories for $[L]^{3+}$ (a), $[Ag_4L]^{3+}$ (b) and $[ZnL]^{3+}$ (c).[17]

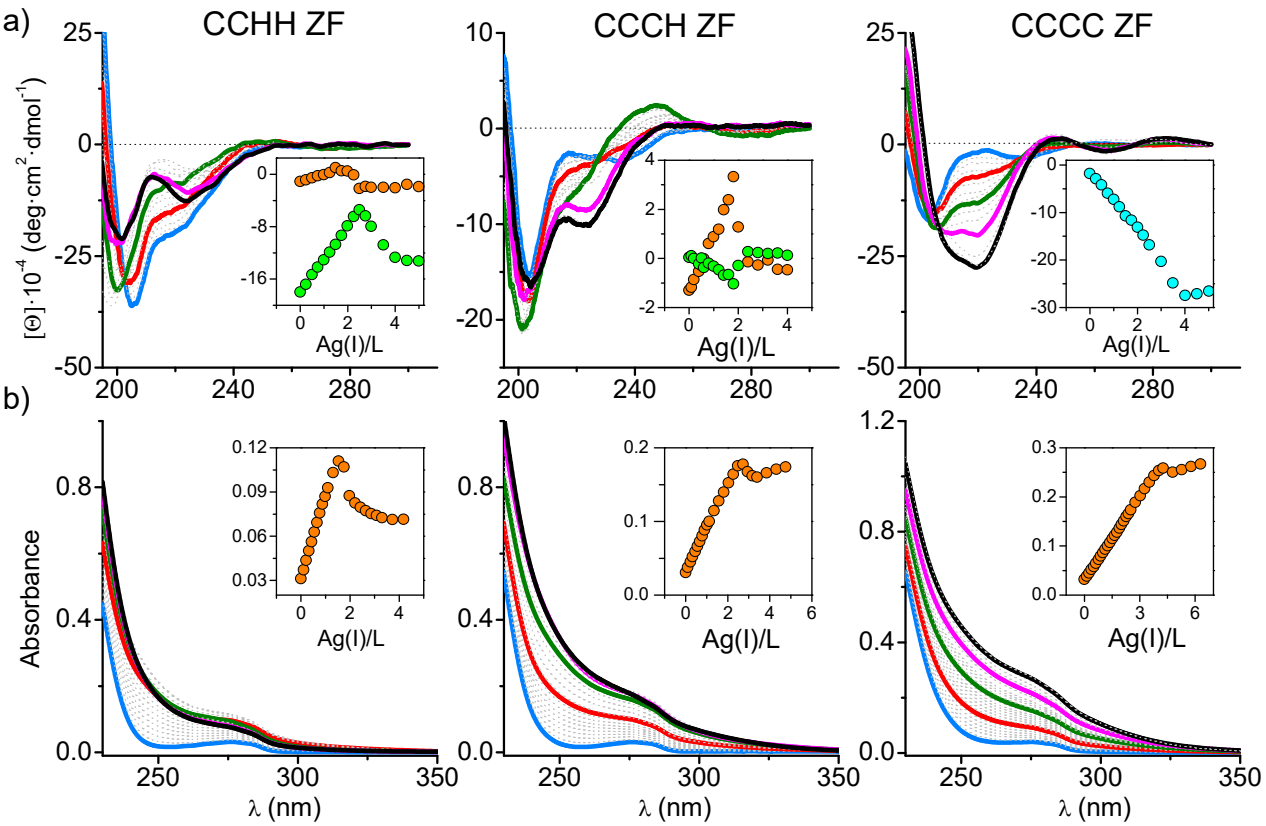

Figure S10. Spectroscopic competition titrations of 25 μM ZnZF complexes in 20 mM TES buffer (pH 7.0) with 0 eq. (blue), 1 eq. (red), 2 eq. (green), 3 eq. (magenta) and 4 eq. (black) of Ag(I). (a) Spectropolarimetric competition titration spectra recorded for ZnZFs. The inset show the changes in molar ellipticity at 247 nm (orange) and 224 nm (green) and 220 nm (cyan). (b) Spectrophotometric competition spectra recorded in the UV-Vis range (230–350 nm). The inset show the changes in absorption at 278 nm over the range of 0-4 eq. of Ag(I).

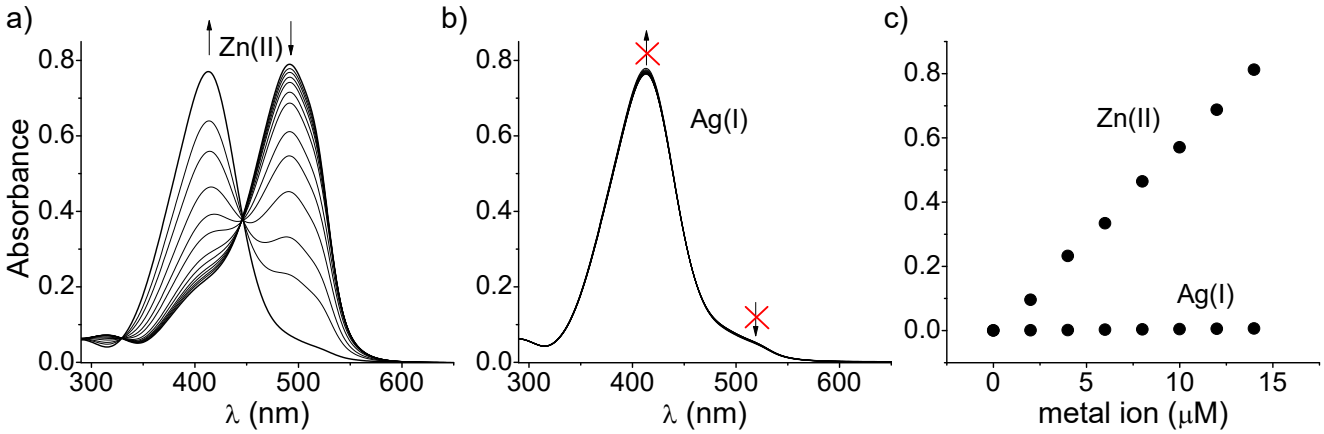

Figure S11. UV-Vis spectra of 20 μM PAR titrated with Zn(II) (a) and Ag(I) (b) in the range of 0-20 μM. (c) Titration of 100 μM PAR with Zn(II) and Ag(I) ions at 492 nm. All titration experiments were obtained in 20 mM TES buffer, pH 7.0.

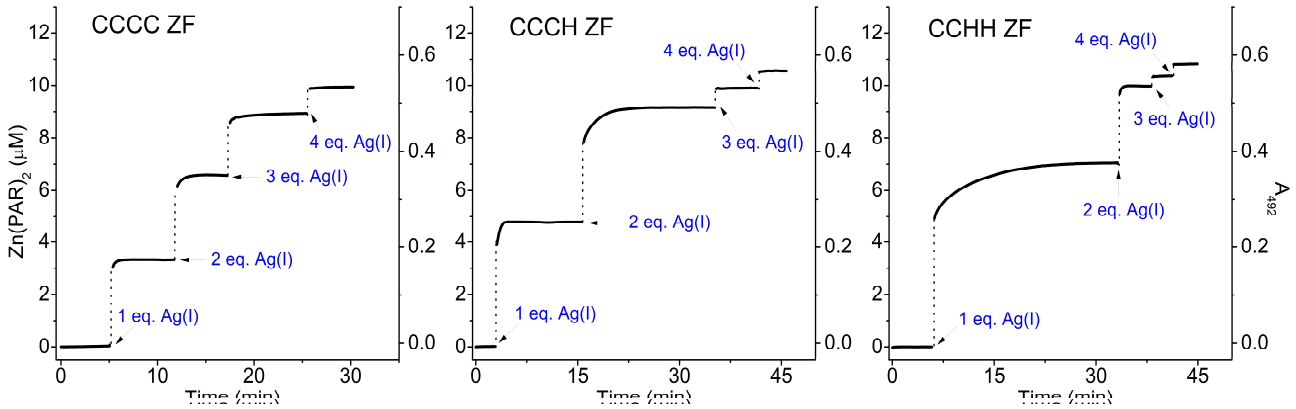

Figure S12. Zn(II) transfer from 10 μM ZFs to PAR observed during titration with 0-4 eq. of Ag(I) measured in 20 mM TES buffer (pH 7.0). After addition of each Ag(I) equivalents samples were equilibrated until appearing curve, connected with Zn(II) to PAR transfer, reached plateau. The $Zn(PAR)_2$ complex concentration was calculated based on PAR absorbances at 492 nm and extinction coefficient at pH 7.0.[1]

Stability constants determination

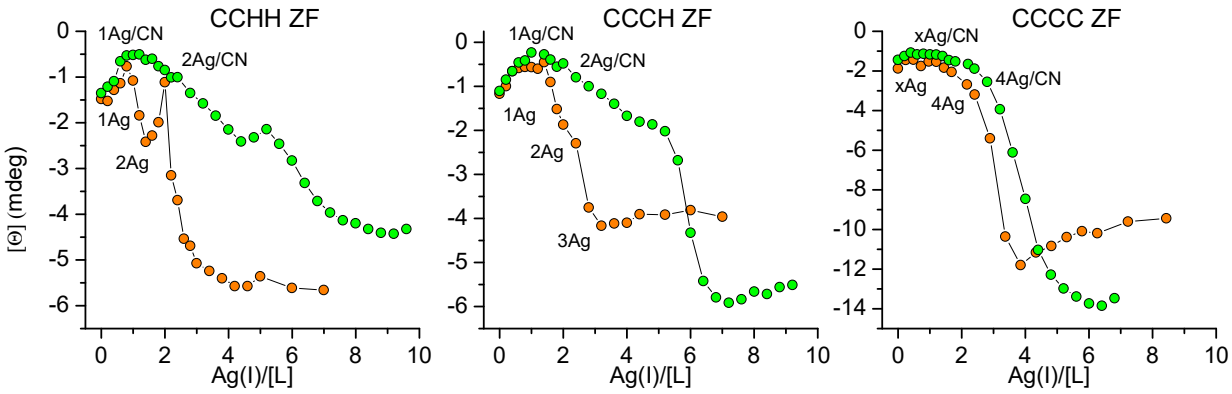

Figure S13. Exploration of silver fingers stability. Spectropolarimetric titration of CCHH, CCCH and CCCC ZF peptides with Ag(I) in the presence (green) and absence (orange) of 150 μM KCN in 20 mM TES buffer (pH 7.0) at 225 nm, 223nm and 220 nm, respectively.

The quantitation of Ag(I) interactions with the ZFs was attempted with the use of cyanide as competing ligand. The log β values reported for $[Ag(CN)_2]^-$ are in the range of 20-21, depending on the source and conditions, as reviewed in the IUPAC report,[24] and confirmed by later studies.[25] We chose the value 20.9, recommended by this report.[26] The monovalent [AgCN] species could be safely ignored due to its low stability.[25] In the calculations of the conditional stability constants the HCN pK_a of 9.06 was used.[27]

The CD signal characteristic of α-helix at 220-225 nm was used to generate the titration data. The complicated shapes of titration curves for CCHH and CCCH fingers both in the absence and presence of cyanide indicate multiple (at least two) stoichiometries of silver complexes of these ZFs, in a comprehensive agreement with the MS data. This precludes a direct determination of Ag(I) affinity to these ZFs. The qualitative analysis of the titrations is presented in Table S7.

Table S7. Locations of titration midpoints in molar equivalent of Ag(I).

Putative species	CCHH	CCCH	CCCC
Species 1, no CN^-	1.1	1.78	3.0
Species 1, with CN^-	2.9	2.86	3.65
Shift	**1.8**	**1.08**	**0.65**
Species 2, no CN^-	2.25	2.67	--
Species 2, with CN^-	6.2	5.8	--
Shift	**3.95**	**3.13**	**--**

The larger the midpoint shift enforced by cyanide, the relatively weaker the Ag(I) complex. The data in Table S7 clearly show the positive correlation between the number of Cys residues in the ZF and the Ag(I) affinity.

Moreover, for the CCHH and CCCH ZFs the lower stoichiometry species (Species 1, presumably AgL for CCHH and AgL/Ag_2L for CCCH based on the midpoint position in the absence of cyanide) are clearly relatively stronger (less shifted) from Species 2. Therefore, the CCHH and CCCH cores do not provide the right environment for cooperative Ag_nS_n cluster formation. In contrast, the complexation of Ag(I) to the CCCC ZF is highly cooperative and only one species prevails in the CD titration. The titration midpoint at 3.0 mol. equiv. of Ag(I) clearly confirms that this species is Ag_4L, in accord with other spectroscopic titrations (Fig. 1 and Fig. 2) and the MS data and modeling. This observation enabled us to make an estimation of the conditional stability constant for this complex at pH 7.0, as follows.

Let us first consider the quantities of species at the titration midpoint. The total reagent concentrations are: CN^-, 150 μM; ZF, 25 μM; Ag(I), 3.65 × 25 = 91.25 μM. At the midpoint half of the ZF is bound in the Ag_4L complex, because the CD signal is quite selective for this complex. Therefore, [Ag_4L] = 12.5 μM, and the amount of Ag(I) ions bound in Ag_4L is 50 μM. Taking the midpoint shift as the measure of $[Ag(CN)_2]^-$ concentration, we obtain 16.25 μM, consuming 32.5 μM of CN^-. The remainder is 117.5 μM CN^-, 12.5 μM ZF and 91.25 – 50 – 16.25 = 25 μM of Ag(I) ions and the 12.5 μM of unaccounted ZF. The latter suggests the exact Ag_2ZF stoichiometry, as the experimental conditions preclude the presence of any unbound Ag(I) ions. However, the other titration experiments suggest that the actual stoichiometry of this species is closer to the equimolar mixture of AgL, Ag_2L and Ag_3L. Assuming the absence of cooperativity in these species of the CCCC ZF, we may attempt to roughly estimate their Ag(I) affinity using the CCCH ZF titration data.

The midpoint of Species 1 in CCCH ZF is at 1.78 mol. eq. of Ag(I), shifted by cyanide to 2.86 mol. eq. The concentrations of reagents are: CN^-, 150 μM; ZF, 25 μM; Ag(I), 1.78 × 25 = 44.5 μM without cyanide and 2.86 × 25 = 71.5 μM with cyanide. Thus the $[Ag(CN)_2]^-$ concentration is 27 μM and free CN^- is 96 μM. Let us simplify the Ag(I)/[L] species mixture as proposed above, by representing it with a single Ag_2L complex, at 22.25 μM, with 2.75 μM of unbound peptide. The log $\beta_{Ag(CN)2}$ = 20.9 includes the deprotonated cyanide, thus the conditional constant ${}^{C}K_{7.0}$, which should be used for calculation at pH 7.0 should be corrected by the cyanide pK_a of 9.06 ($\log {}^{C}K_{7.0} = \log \beta_{Ag(CN)2} - 2 \times (9.06\text{-}7.0) = 16.78$). This yields $[Ag(I)] = [Ag(CN)_2^-]/([CN^-]^2 \times {}^{C}K_{7.0}) = 2.7 \times 10^{-5} / (9.2 \times 10^{-9} \times 6.0 \times 10^{16}) = 4.9 \times 10^{-14}$ M. [Ag(I)] can now be substituted to the formula for the apparent Ag_2L complex: $K_{Ag2L} = [Ag_2L]/([Ag(I)]^2 \times [L]) = 2.225 \times 10^{-5} / 2.4 \times 10^{-27} \times 2.75 \times 10^{-6} = 3.4 \times 10^{27}\ M^{-2}$ which can be translated as $5.8 \times 10^{13}\ M^{-1}$ per Ag(I) (K_d of 17.2 fM).This value can be positively cross-checked against the data for simpler thiol ligands, e.g. 2-mercaptoethanol, 3-mercaptopropanol and monothiopentaerythritol, for which log$K$ values of 12-13 were reported.[28,29]

The affinity of the Ag_4L complex of the CCCC ZF can now be estimated via the Ag_2L/Ag_4L equilibrium: $Ag_2L + 2\ Ag^+ = Ag_4L$. At the midpoint of the titration $K_{Ag2L/Ag4L}$, defined as $[Ag_4L]/([Ag(I)]^2 \times [Ag_2L]$ is reduced to $1/[Ag^+]^2$. This value can be obtained directly from ${}^{C}K_{7.0}$, substituting $[CN^-] = 117.5$ μM and $[Ag(CN)_2]^- = 16.25$ μM. The resulting $K_{Ag2L/Ag4L} = 2.5 \times 10^{27}\ M^{-2}$, leading to $K_{Ag4L} = K_{Ag2L/Ag4L} \times K_{Ag2L} = 2.5 \times 10^{27}\ M^{-2} \times 3.4 \times 10^{27}\ M^{-2} = 8.5 \times 10^{54}\ M^{-2}$, which corresponds to $5.4 \times 10^{13}\ M^{-1}$ per Ag(I) (K_d of 18.5 fM). These values should be treated as lower estimates, rather than the accurate determinations of the Ag(I) affinity to ZF proteins, due to the nature of necessary simplifications used in our calculations.

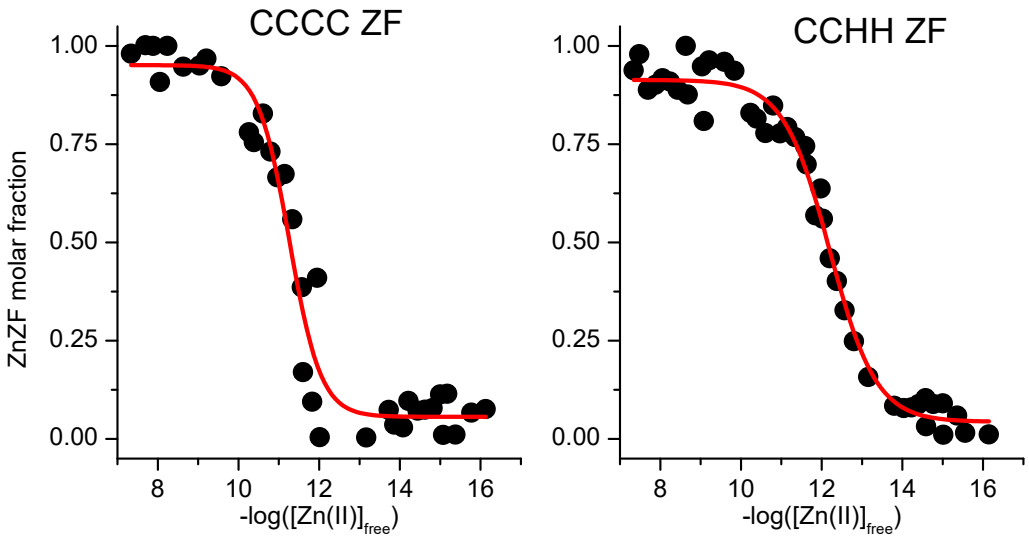

Figure S14. Isotherms of Zn(II) binding to CCCC and CCHH ZF peptides in a set of metal buffers in 20 mM TES buffer (pH 7.0). Fraction of the ZF complex was calculated based on CD changes in the applied $\log[Zn(II)]_{free}$ range.

Table S8. Comparison of log*K* values determine for Zn(II) and Ag(I) ZF complexes.

Zinc finger	$\log K_{ZnL}$	$\log K_{AgL}$[a]	$\log K_{AgL}$[a] - $\log K_{ZnL}$
CCHH	12.20 ± 0.05	13.8	1.6
CCCC	11.26 ± 0.07	13.7	2.4

[a] K_{AgL} refers to the average value for a single Ag(I) ion in K_{Ag2ZF} and K_{Ag4ZF} clusters)

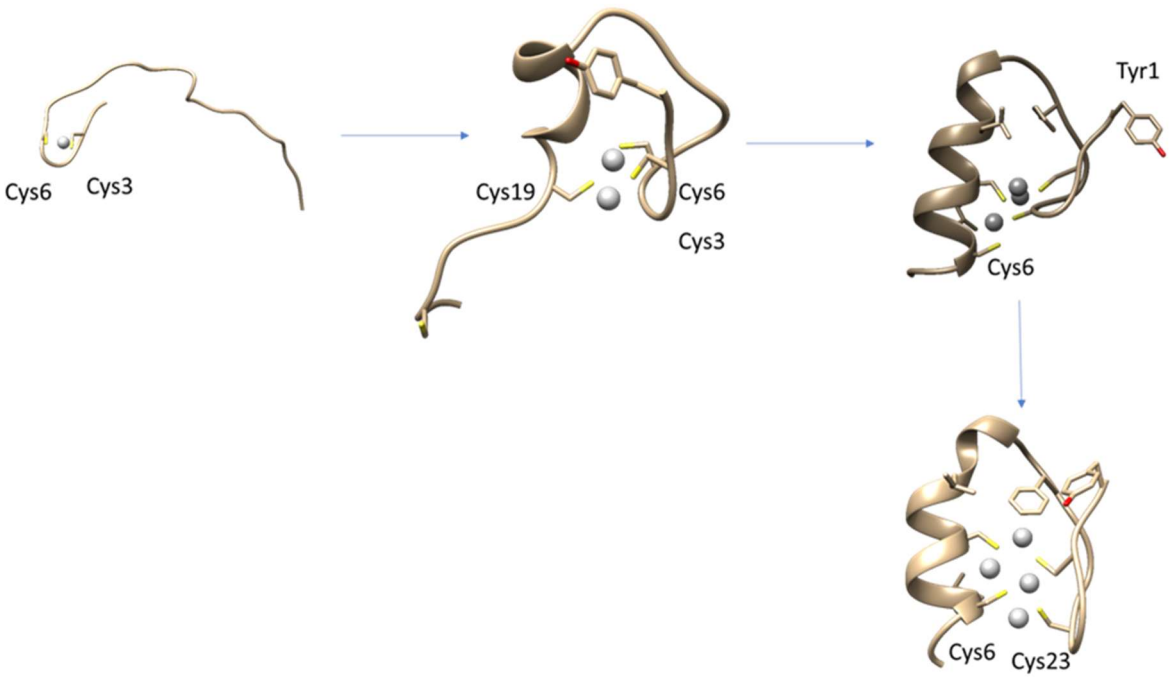

Figure S15. Schematic representation of the metal-coupled folding process of CCCC ZF peptide.

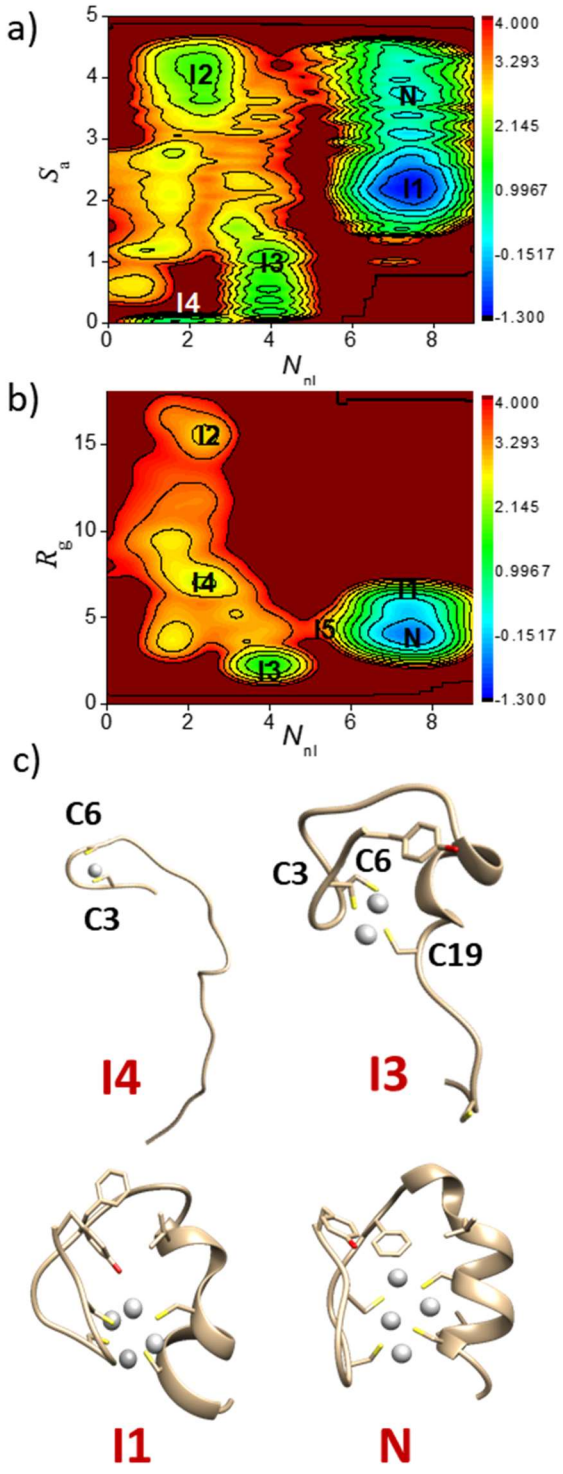

Figure S16. Free energy surfaces of CP1 peptide folding obtained by WT-MetaD. The free energy projected onto collective variables (a) (Sα, N_{nl}) and (b) (R_g, N_{nl}). The basin labelled as N, I1-I5 corresponds to native state and intermediates, respectively. (c) Average structures for the basins I1, I3-4 and N are shown. The S_α, N_{nl}, R_g denote number of backbone-backbone α-helical hydrogen bonds formed between Ser15-Cys19, number of native coordination bonds formed between Cys residue and Ag(I) and radius of gyration of the hydrophobic core characterized by side chain carbon atoms from Tyr1, Phe10 and Leu16 residues, respectively.

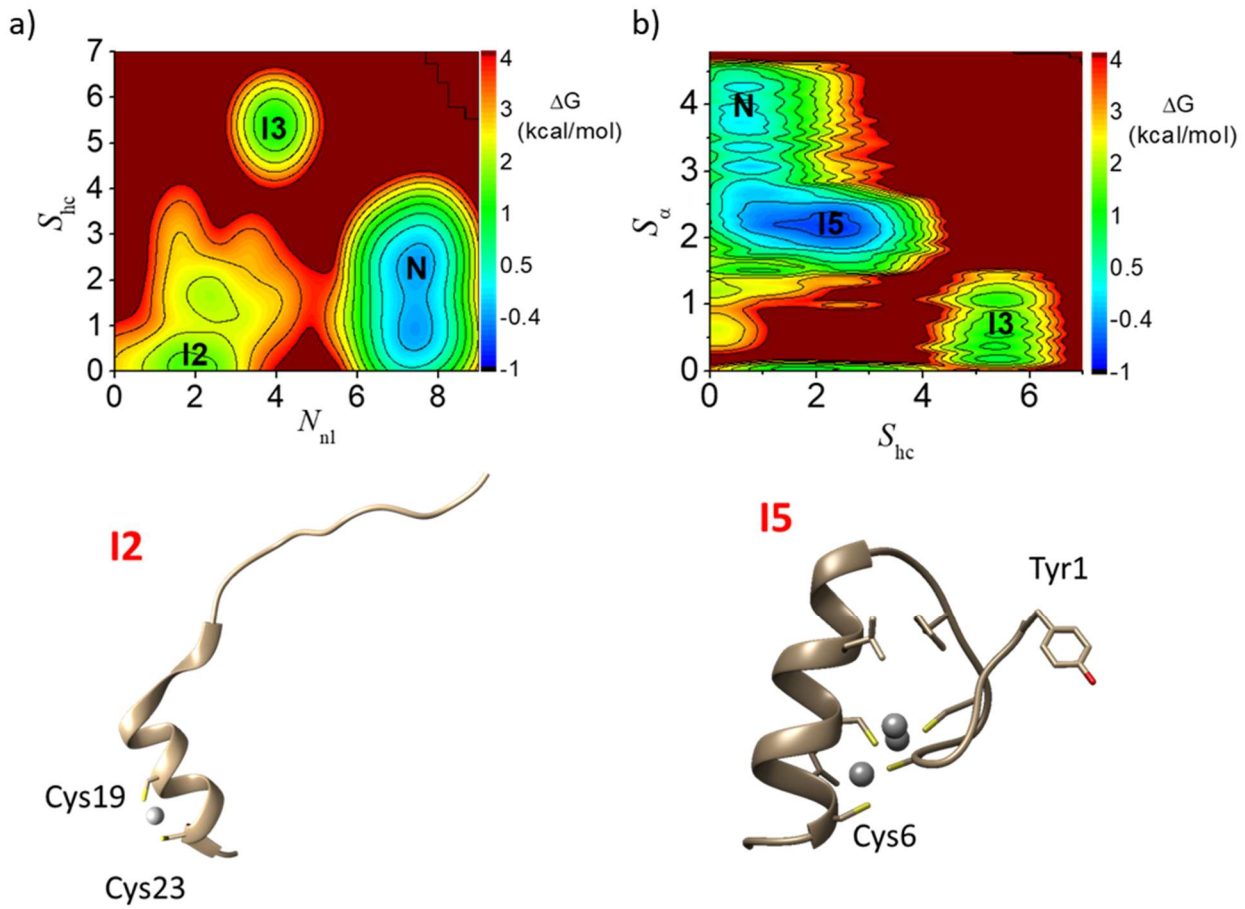

Figure S17. Free energy surfaces of CCCC ZF peptide folding obtained by WT-MetaD. The free energy projected onto collective variables (S_{hc} vs. N_{nl}) (a), (S_α vs. S_{hc}) (b). The basin labelled as N, I1, I2, I3, I5 corresponds to native state and intermediates, respectively. Basins corresponding to intermediates (I) indicated in the free energy surfaces are shown. Basins corresponding to native state (N) and intermediates (I) indicated in the free energy surfaces from Figure S15. The S_α, S_{hc} and N_{nl}, are defined as the number of backbone-backbone α-helical hydrogen bonds formed between Ser15-Cys19, the number of contacts in the hydrophobic core formed by Tyr1, Phe10 and Leu16 and the number of native coordination bonds formed between Cys residue and Ag(I), respectively.

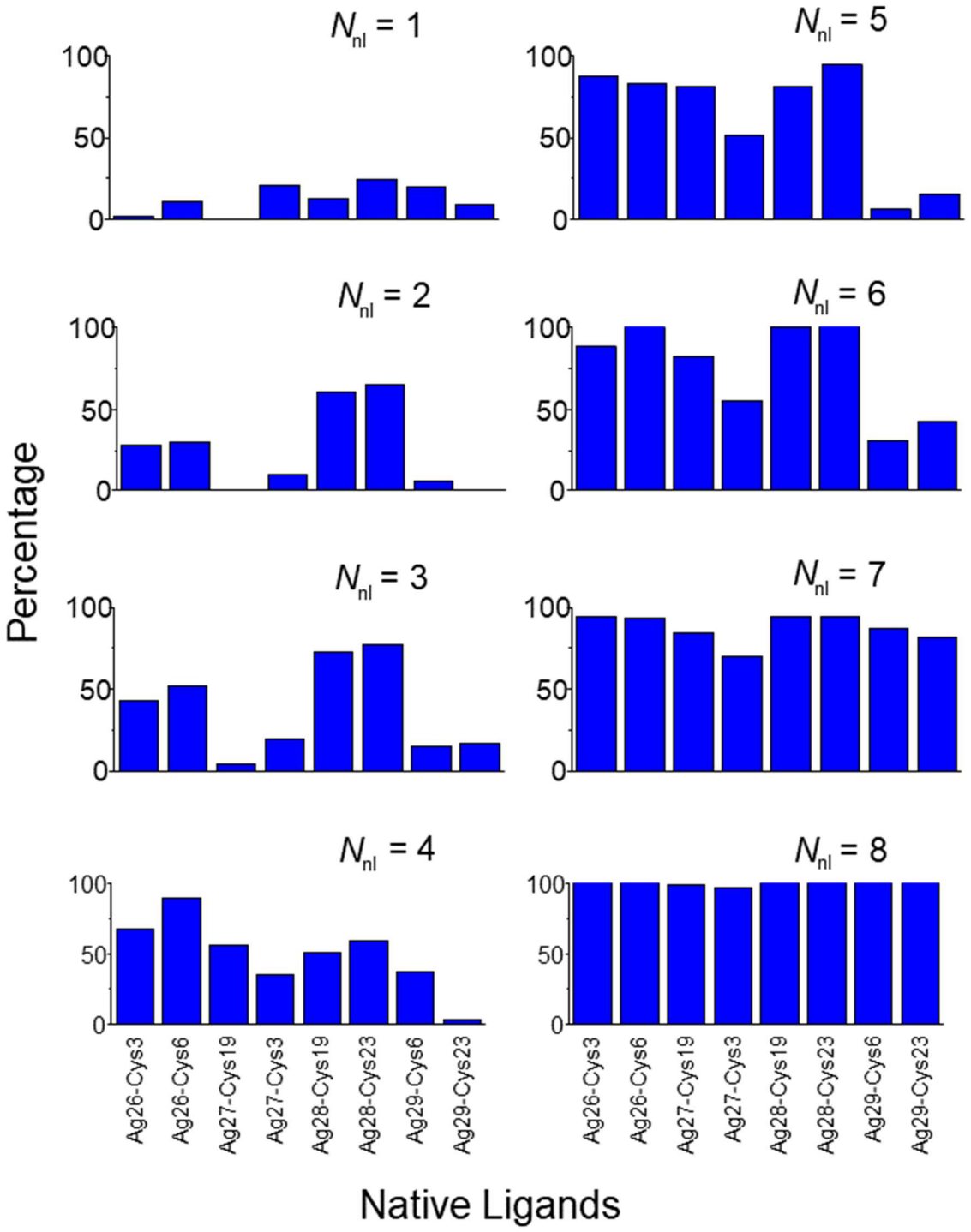

Figure S18. Percentages of formation of the eight native coordination bonds with one to eight native coordination bonds formed. N_{nl} is the number of native coordination bonds formed. In the binding order analysis of native ligands, we observe that unstable intermediate with Cys19-Ag(I)-Cys23 and Cys6-Ag(I)-Cys3 might be form but we did not observe a basin in any FES assayed (Fig. S16-17).

References

1 A. Kocyła, A. Pomorski, A. Krężel. *J. Inorg. Biochem.* 2015, **152**, 82–92.

2 A. Krężel, J. Wójcik, M., Maciejczyk, W. Bal. *Inorg. Chem.* 2011, **50**, 72–85.

3 A. Pomorski, T. Kochańczyk, A. Miłoch, A. Krężel. *Anal. Chem.* 2013, **85**, 11479–11486.

4 A. Krężel, R. Latajka, G.D. Bujacz, W. Bal. *Inorg. Chem.* 2003, **42**, 1994–2003.

5 K. Kluska, J. Adamczyk, A. Krężel, *Coord. Chem. Rev*. 2018, **367**, 18–64.

6 T. Kochańczyk, M. Nowakowski, D. Wojewska, A. Kocyła, A. Ejchart, W. Koźmiński, *Sci. Rep*. 2016, **6**, 36346.

7 A. Miłoch, A. Krężel, *Metallomics* 2014, **6**, 2015–2024.

8 T. Kochańczyk, P. Jakimowicz and A. Krężel, *Chem. Comm*. 2013, **49**, 1312–1314.

9 K. Kluska, J. Adamczyk, A. Krężel, *Metallomics,* 2018, **10**, 248-263.

10 A. Krężel, W. Maret, *Arch. Biochem. Biophys.* 2016, **611**, 3–19.

11 L. Alderighi, P. Gans, A. Ienco, D. Peters, A. Sabatini, A. Vacca, *Coord. Chem. Rev*. 1999, **184**, 311–318.

12 K. M. Hines, J. C. May, J. A. McLean, L. Xu, *Anal. Chem.* 2016, **88**, 7329–7336.

13 M. F. Bush, I. D. G. Campuzano, C. V. Robinson, *Anal. Chem.* 2012, **84**, 7124–7130.

14 B.T. Ruotolo, J. L. P. Benesch, A. M. Sandercock, S. J. Hyung, C. V. Robinson, *Nat. Protoc.* 2008, **3**, 1139–1152.

15 M. F. Bush Z. Hall, K. Giles, J. Hoyes, C. V. Robinson, B. T. Ruotolo, *Anal. Chem.* 2010, **82**, 9557–9565.

16 K. Thalassinos, M. Grabenauer, S. E. Slade, G. R. Hilton, M. T. Bowers, J. H. Scrivens, *Anal. Chem.* 2009, **81**, 248–254.

17 G. Marklund, M. T. Degiacomi, C. V. Robinson, A. J. Baldwin, J. L. P. Benesch, *Structure* 2015, **23**, 791–799.

18 B. Webb, A. Sali. Comparative Protein Structure Modeling Using Modeller. Current Protocols in Bioinformatics 54, John Wiley & Sons, Inc. 2016, 5.6.1-5.6.3.

19 D. A. Case, T. E. Cheatham III, T. Darden, H. Gohlke, R. luo, J.R. K. M. Merz, A. Onufriev, C. Simmerling, B. Wang, R. J. Woods, *J. Comput. Chem.* 2005, **26**, 1668–1688.

20 S. Pronk, S. Pall, R. Schulz, P. Larsson, P. Bjelkmar, R. Apostolov, M.R. Shirts, J.C. Smith, P. M. Kasson, D. van der Spoel, B. Hess, E. Lindahl, *Bioinformatics* 2013, **29**, 845–854.

21 G.A. Tribello, M. Bonomi, D. Branduardi, C. Camilloni, G. Bussi, *Comput. Phys. Commun*. 2014, **185**, 604–613.

22 P. Hosek and V. Spiwok, *Comput. Phys. Commun.* 2016, **198**, 222–229.

23 A. Barducci, G. Bussi, M. Parrinello. *Phys. Rev. Lett.* 2008**, 100**, 020603.

24 M. T. Beck, *Pure & Appl.Chem.* 1987, **59**, 1703–1720.

25 J. H. Kyle, The Australasian Institute of Mining and Metallurgy Publication Series No. 2/97, 1997.

26 R. D. Hancock, N. P. Finkelstein, A. Evers, *J. Inorg. Nucl. Chem.* 1972**, 34**, 3747–3751.

27 V. Gáspár, M. T. Beck, *Acta Chim.Hung*. 1982, **110**, 425–427.

28 K. Tunaboylu, G. Schwarzenbach, *Helv.Chim.Acta*. 1971, **54**, 2166–2185.

29 N. Adams, J. Kramer; *Aquatic Geochem.* 1999, **5**,1–11.